Proceedings of the ASME 2023
International Design Engineering Technical Conferences &
Computers and Information in Engineering Conference
IDETC-CIE 2023
August 20–23, 2023, Boston, MA

IDETC-CIE2023-117184

DATA FUSION COGNITIVE COMPUTING FOR CHARACTERIZATION OF MECHANICAL PROPERTY IN FRICTION STIR WELDING PROCESS

Danny Hoang[1], Ruimin Chen[1], Debasish Mishra[2], Surjya K Pal[3], Farhad Imani[1]*

[1]Department of Mechanical Engineering, University of Connecticut, Storrs, CT
[2]UTC Institute for Advanced Systems Engineering, University of Connecticut, Storrs, CT 06269, USA
[3]Department of Mechanical Engineering, Indian Institute of Technology Kharagpur, Kharagpur, West Bengal, India

ABSTRACT

High intricacy of the friction stir welding (FSW) process and severe plastic deformation typically result in serious part quality concerns, including thinning, groove, and kissing bond. These defects, in turn, impact mechanical properties (e.g., Young's modulus and yield strength), thereby deteriorating the performance of a joint part. Machine learning methods such as feature-based support vector machines and end-to-end deep neural networks are recently coupled with in-situ sensing to link process parameters with the final properties, yet the low accuracy and precision, poor sample efficiency, and lack of interpretable learning limit their capabilities for reliable characterization. This research introduces hyperdimensional cognitive computing (HCC) that mimics human brain functionalities to fuse power, torque, and force data and provide robust, sample-efficient, and explainable learning for process-property characterization in FSW. Data augmentation is integrated with HCC to tackle the imbalanced data problem. The experimental results show that HCC seamlessly fuses in-situ data to predict the ultimate tensile strength with an F1-score of 0.899 ± 0.048*, which is 21.579%, 47.779%, 1.933%, and 68.139% better than support vector machine, logistic regression, Naive-Bayes and multilayer perceptron, respectively. Besides the superior prediction capability, HCC symbolic representation reveals that measured force is the critical factor in the characterization of ultimate tensile strength. The proposed HCC is shown to be effective for data fusion and single-pass learning and eliminates the necessity of costly and long retraining in various manufacturing processes such as 3D printing and bio-fabrication.*

Keywords: Friction stir welding, Cognitive computing, Data fusion, Property characterization

*Corresponding author: farhad.imani@uconn.edu

1. INTRODUCTION

Friction stir welding (FSW) has drawn increasing attention for efficient manufacturing in several domains, including aerospace [1], shipbuilding [2], railways [3], and automobiles [4]. Unlike conventional welding techniques that are limited to single substrate metal material and face concerns of hot cracks and coarse grains, FSW welds dissimilar workpieces in a solid state using a non-consumable tool [5], which offers a path to lower temperature with no pollution joining.

During an FSW process, two base materials are welded together. One side is called advancing, while the other is named the retreating side. On the advancing side, the rotation vector's direction is comparable with the welding direction, and this is the opposite on the retreating side. During fabrication, a durable rotating tool with a tailored designed pin and shoulder is placed at the abutting edges of two substrates to join them. As the tool travels over the joint line, the created thermal energy in the stir zone due to the friction between the workpiece and the shoulder leads to the permanent change of the materials [6]. This contributes to the deformation of material alongside the verge of the tool, further forming various defects in the weld joint.

During the fabrication, process, design, and material parameters are closely related to weld quality. Process parameters, e.g., plunge depth p, tilt angle α, welding speed ν, and rotational speed ω can be controlled online. On the other hand, design parameters, e.g., height of pin, diameter of shoulder, diameter of pin, and material parameters, are mainly offline controllable. With these parameters that are associated with the quality of outcome, defects in FSW can be linked into three categories: excessive heating, insufficient heating, and design flaws [7]. Excessive heating happens with high rotational speed, high tilting angle, high plunge depth, and low welding speed, which often result in the melting of substrate materials [8]. Under improper technological conditions, process parameters, or welding tools,

mechanical properties can be quickly deteriorated through the formation of welding defects. For example, a larger plunge depth or intensive welding heat input not only creates flash flaws but also causes stress concentration along with weld thinning anomalies. The lower heat input because of inadequate material flow raises the possibility of internal defects, including groove, tunnel, and cavity. Even though the tunnel and kissing bond are impacted by the plunge offset and depth, adjusting processing parameters (e.g., tilt angle, processing speed, rotational velocity, and plunge force), can improve defect formation and mechanical properties.

As such, advanced sensing is implemented with the FSW process to capture diverse in-situ quality signatures through measuring power, torque, force, and acoustic emission signals. Machine learning (ML) methods are integrated to characterize the relationship between the process parameters and optimize the welding setup that is essential to fabricating high-quality joints. For instance, [9] implemented wavelet and Hibert-Huang transforms to combine the force signal and then predicted the strength of the weld joint using support vector machines (SVM). [10] designed a monitoring scheme for FSW by signal decomposition of torque of spindle motor with Fourier transformation. The development of tunnels or voids in welding is attributed to signal variation. [11] evaluated the ultimate tensile strength (UTS) through multilinear regression, SVM, and Gaussian process (GP). Out of 25 data, 19 were chosen to train and test models. Here, rotational speed and feed rate took into account as input variables. The result shows that the Gaussian process has superior performance in comparison with two other methods. [12] designed a monitoring technique according to SVM and optical images of weld surfaces. The features from images were captured through a maximally stable extremal regions algorithm to differentiate the good and bad welding. Recently, end-to-end artificial neural networks (ANNs) have been implemented to account for the non-linearity of input variables. [13] applied deep learning neural network to map the ultimate tensile strength according to the shoulder diameter, tool transverse speed, tool tilt, and pin diameter with 119 experimental data from copper material. [14] leveraged recurrent, feedforward, and convolutional neural networks to determine the quality of surface welded parts. [15] investigated ANN to model the vital process parameters on the quality of parts using thirty AA-7075-T6 specimens. The input parameters include pin diameter, and axial forces, together with tool hardness, and outputs consist of notch tensile strength and welding zone hardness. [16] utilized decision tree regression, random forest, and artificial neural network to estimate the tensile behavior associated with aluminum alloy in FSW. The observation suggested that random forest performs prediction of the tensile strength with higher accuracy.

The generated data from diverse measurement sources such as force, torque, and power in FSW often leads to multi-channel data with complex dynamics, thereby preventing efficient knowledge extraction in traditional AI methods such as SVM and GP. Although ANNs can tackle this problem and autonomously learn hierarchies of features of multi-channel time series through backpropagation with several units, including fully connected layers, pooling layers, and convolution layers, the presence of limited training samples prevents practical learning. The small sample size introduces bias into the learning since prevents millions of weights from being updated accurately through backpropagation [17, 18].

One of the potential solutions to deal with these challenges is seeking cognitive power and utilizing it alongside ML systems. Cognitive is defined as the art of thinking, reasoning, and remembering. The term cognitive science means the perception of humans, the way a human thinks, learns, and performs tasks with a few supervised instances. Leveraging human skills and experiences for knowledge discovery is known as cognitive intelligence [19–21]. In this paper, we communicate the development and implementation of cognitive computing in FSW that various process signatures are captured. Specifically, we have developed hyperdimensional computing (HCC) framework for fusing multi-channel data and characterizing the mechanical properties of FSW. HCC originated through the abstract representation of neuronal circuits in the human cerebrum. It mimics the use of cognitive skills in making decisions through leveraging various brain-related mathematical notions for efficient hot vector operations (more than 10000 bits) [22–24]. Hence, HCC retains memory to reduce computational costs and enable learning with limited data. Furthermore, HCC vectors, by nature, are extremely robust against noise, much like the human's central nervous system. Intelligence requires detecting, storing, binding, and unbinding noisy patterns, and HCC is well-suited to handling noisy patterns. As it is motivated by the neuronal circuits present in the human neural system, HCC architecture involves encoding, training, and comparison stages. We show augmentation of the sensors to balance it and fusion of data to derive meaningful and accurate information.

The remainder of this paper is organized as follows: Section 2 introduces the proposed HCC framework. Section 3 discusses the detailed setup of the FSW experiments. Section 4 illustrates experimental results. Finally, this study is concluded in Section 5.

2. METHODOLOGY

The objective of this research is to characterize the ultimate tensile strength of the FSW through in-process multi-channel measurements and the paradigm of cognitive data fusion computing. As illustrated in Figure 1, multiple process data, i.e., power, torque, and force, are collected by different sensors that are integrated with the Montronix PS100 FSW machine. Then, we determine the UTS for each specimen after fabrication and classify each specimen into different categories. Next, we perform several sampling strategies and data augmentation to the collected data to balance each category for further analysis. The proposed hyperdimensional cognitive computing is analyzed to evaluate the capability of the framework. Finally, HCC is compared with other state-of-the-art machine learning models to verify superior performance and interpretability in characterization.

2.1 Hyperdimensional Cognitive Computing

HCC first encodes the training data into the high-dimensional space. Then, HCC generates a hypervector in the length of thousands to represent each class and perform learning over the encoded data through single-pass training. Next, by comparing the similarity between class hypervectors and encoded query data, HCC is retrained to assign the closest class to the query.

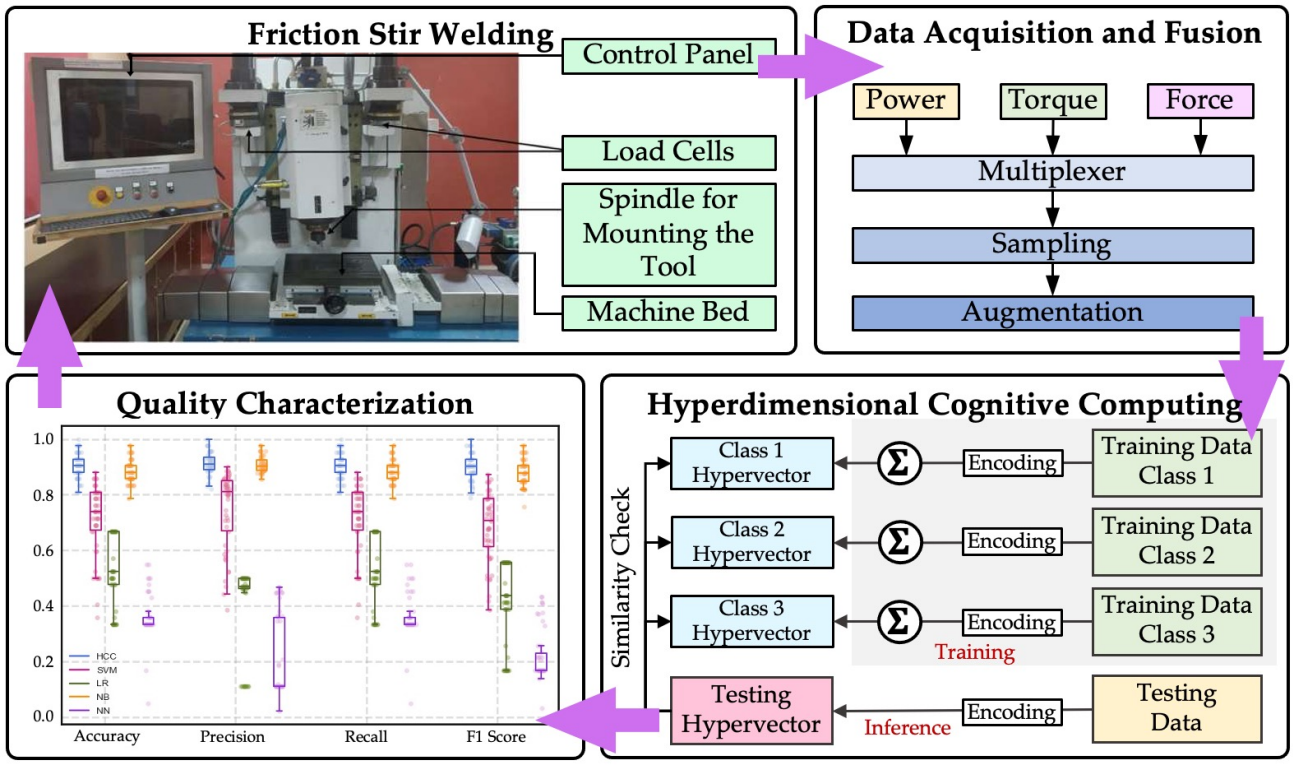

FIGURE 1: FLOWCHART OF THE PROPOSED METHODOLOGY FOR DATA FUSION AND COGNITIVE COMPUTING FOR CHARACTERIZATION OF MECHANICAL PROPRIETIES IN FSW PROCESS.

2.1.1 Encoding. Let assume we denote dataset as $\mathbf{X} = \{\mathbf{x}_1, \mathbf{x}_2, ..., \mathbf{x}_N\}$, and their corresponding label set as $\mathbf{y} = \{y_1, y_2, ..., y_N\}$, where N represents the number of instances. The objective of encoding is to map the dataset to the hypervector set $\mathbf{H} = \{\mathbf{H}_1, \mathbf{H}_2, ..., \mathbf{H}_N\}$. Assume each vector $\mathbf{x}_n \in \mathbf{X}$ has M features, i.e., $\mathbf{x}_n = \{x_{n1}, x_{n2}, ..., x_{nM}\}$. Our goal is to encode time series data $\mathbf{x}_n$ into the large-dimensional space. We encode the data as $\mathbf{H}_n = \{h_{n1}, h_{n2}, ..., h_{nD}\}$, where $h_{ni} \in \{0, 1\}\, \forall i \in 1, ..., D$. We assume a set of randomly selected orthogonal bipolar base hypervectors $\mathbf{B} = \{\mathbf{B}_1, \mathbf{B}_2, ..., \mathbf{B}_M\}$, where $\mathbf{B}_i\, \forall i \in 1, ..., M$ has the same dimensionality of hypervector (i.e., D). Since each element of $\mathbf{B}$ is randomly created from streams of bit, the similarity between two base hypervectors is nearly orthogonal. In other words, $\delta(\mathbf{B}_i, \mathbf{B}_j) \simeq 0 \quad (0 < i, j < M, i \neq j)$. The encoding procedure can be represented as

$$h_{ni} = \cos(\mathbf{x}_n \cdot \mathbf{B}_i^T + b_i) \times \sin(\mathbf{x}_n \cdot \mathbf{B}_i^T) \tag{1}$$

where each element of $\mathbf{B}_i$ follows standard Gaussian distribution (i.e., mean 0 and standard deviation 1). The b_i is a random sample from a uniform distribution in range of $[0, 2\pi]$. Note that the basis function $\mathbf{B} = \{\mathbf{B}_1, \mathbf{B}_2, ..., \mathbf{B}_M\}$ can be generated once at the beginning of the training. The calculated $\mathbf{H}_n$ for data $\mathbf{x}_n$ has non-binary values. Therefore, the hypervector is binarized using the sign function as $\mathbf{H}_n = \text{sign}(\mathbf{H}_n)$. The sign function places the value +1 for positive dimensions of hypervector and −1 to all non-positive elements.

Here, the perpendicularity of hypervectors is guaranteed by the size of the hypervector being large enough to compress with the size of feature vectors in the original data, i.e., $D >> M$. For a different type of data (i.e., power, torque, and force), different encoding methods will be implemented, where the encoding criteria are to let the data vectors that are different from another in the original space also be orthogonal in the hyperspace. For the scenario where multiple sensors are involved, the proposed encoder follows the same procedure for each sensor using the synchronized n-gram windows. For example, assume there is S number of sensors integrated with the system, and the sensors generate a set of encoded hypervectors $\{\mathbf{H}^1, \mathbf{H}^2, ..., \mathbf{H}^S\}$. We accordingly generate a set of random hypervectors $\{\mathbf{P}^1, \mathbf{P}^2, ..., \mathbf{P}^S\}$, where each $\mathbf{P}$ represents a signature of a sensor. As the next step, hypervectors from each sensor will be bound with the associated identification hypervector to aggregate the information, i.e., $\mathbf{H} = \mathbf{P}^1 \times \mathbf{H}^1 + \mathbf{P}^2 \times \mathbf{H}^2 + ... + \mathbf{P}^S \times \mathbf{H}^S$.

2.1.2 Single-pass Learning. Next, a linear training module is incorporated to combine the encoded hypervectors from each class to find the universal property for training data. Specifically, hypervectors are appended from the same class to create a single class hypervector. However, instead of adding all encoded hypervectors together in the conventional single-pass training, the HCC framework joins the encoded data based on the amount of new information appended to the class hypervectors. If a pattern already exists in a class hypervector, the proposed framework only adds a small portion to eliminate model saturation. As such, the HCC is capable of efficient and accurate training with data from multiple sources.

Let $\mathbf{K}_c = \{k_{c1}, k_{c2}, ..., k_{cD}\}$ be the corresponding class hypervector c and $\mathbf{H}_{N+1}$ be an encoded incoming training data. The

HCC framework calculates the similarity between $\mathbf{K}_c$ and $\mathbf{H}_{N+1}$ as

$$\delta(\mathbf{K}_c, \mathbf{H}_{N+1}) = \frac{\mathbf{K}_c \cdot \mathbf{H}_{N+1}}{\|\mathbf{K}_c\| \cdot \|\mathbf{H}_{N+1}\|} \tag{2}$$

where the nominator is the inner product between the class hypervector $\mathbf{K}_c$ and the query $\mathbf{H}_{N+1}$. The closer the δ is to 1, the more similarity exists between two hypervectors.

2.2 Time Series Data Augmentation

Friction stir welding data corresponding to mechanical properties are relatively small due to the high cost of experimentation. Severe imbalances (i.e., concerning the different levels of mechanical properties outcomes in experiments) pose another significant challenge for many supervised models. In other words, as the balance in quantity of training data for each class trespasses, the model trains toward the dominant classes, leading to poor performance for the classes with limited data. Here, we leverage jittering for data augmentation [25]. Assume a time series vector $\mathbf{x}_n \in \mathbf{X}$, the jittering procedure can be represented as

$$\mathbf{x}_n^{'} = \mathbf{x}_n + \boldsymbol{\epsilon}_n \tag{3}$$

where $\boldsymbol{\epsilon}_n \sim \mathcal{N}(\mathbf{0}, \boldsymbol{\Sigma})$. This method creates new data according to the fact that patterns in training and testing samples vary just by a noise factor. Overall, data augmentation enables overcoming the challenge of sparse data and can support the construction of a large dataset for training a robust model.

3. EXPERIMENTAL SETUP

Sheets made of AA6061 aluminum alloy with the dimension of 100 mm × 80 mm × 3 mm are selected as the base material for the FSW experiment. The tool employed for fabricating the weld specimens is an H13 steel material with a conical pin with 6 mm upper diameter, 4 mm lower diameter, and a 2.7 mm of pin length, and a flat shoulder of 18 mm diameter. The numerically controlled FSW machine (i.e., WS004) by ETA technology was chosen to provide the platform for welding the sheets in a butt joint configuration. Note that the WS004 machine has a maximum rate ω of 3000 rpm and maximum rate ν of 1000 mm/min, respectively. There is a control panel attached to the machine where process parameters such as welding speed, rotational speed, starting and ending points, plunge depth, and tile angle are taken as inputs. Here, the spindle head is manually adjusted and set prior to the fabrication process. Therefore, the tilt angle does not change during the fabrication. Also, the depth plunge is fixed by mounting the tool downwards manually. Particularly, the tilt angle is set to be 2° and the depth of plunge as 0.2 mm to achieve defect-free welds.

Rotational speed ω (rpm)	600, 1000, 1400, 1800, 2200, 2600
Welding speed ν (mm/min)	40, 50, 60, 80, 100, 150, 200

TABLE 1: A FULL FACTORIAL EXPERIMENT WITH VARIOUS COMBINATIONS OF ROTATIONAL AND WELDING SPEEDS.

To incorporate analytics in the scheme, sensory data and weld quality are collected and tested comprising various parametric combinations. Specifically, we designed a full factorial

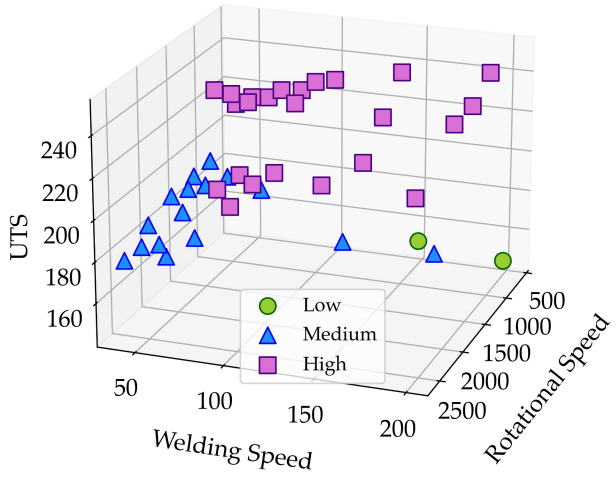

FIGURE 2: UTS VALUES CORRESPONDING TO VARIOUS PARAMETRIC COMBINATIONS.

experiment (see Table 1) to fabricate in total of 42 specimens with rotational speeds (i.e., ω) of 6 levels and welding speeds (i.e., μ) of 7 levels. During the fabrication, torque and force information are acquired via a strain gauge type load cell of the WS004 machine, and a Montronix PS100 Hall-Effect type sensor is integrated with the machine control unit to collect power data. To synchronize the acquisition frequency between different sensors incorporated with the system, the acquisition rate of all sensors is set to be 10 Hz using a data acquisition card (NI 6211), as the FSW machine has a fixed acquisition rate of 10 Hz when collecting force and torque data. For each specimen, one power signal, two torque signals (i.e., X torque and spindle torque), and two force signals (i.e., Z load and X load) are collected.

After fabrication, a post-weld study is performed, and the ultimate tensile strength is determined for each specimen. First, each specimen is cut in the direction that is perpendicular to the weld with a length of 100 mm following the ASTM E8 standard using a CNC wire cut electrical discharge machining (Elektra Maxicut 523). Then, the ultimate tensile strength of each specimen is tested by Instron 8862 universal tensile testing machine. Note that the capacity of the tensile testing machine and the crosshead speed for testing are 100 kN and 1mm/min, respectively. Among the specimens fabricated with the parameters specified in Table 1, the maximum UTS of 249.4 MPa is observed when the rotational speed ω is 1000 rpm and the welding speed ν is 200 mm/min, and the minimum UTS of 146.2 MPa is observed at ω = 600 rpm and ν = 200 mm/min. Further, we categorize the welding specimens according to their UTS values based on the following criteria:

- Low tensile strength (Poor quality weld, labeled as Low): Tensile strength below 162 MPa, i.e., the range corresponds to 0% to 60% of the base material's strength.
- Medium tensile strength (Mid quality weld, labeled as Medium): Tensile strength between 162 and 199.8 MPa, i.e., the range corresponds to 60% to 74% of the base material's strength.

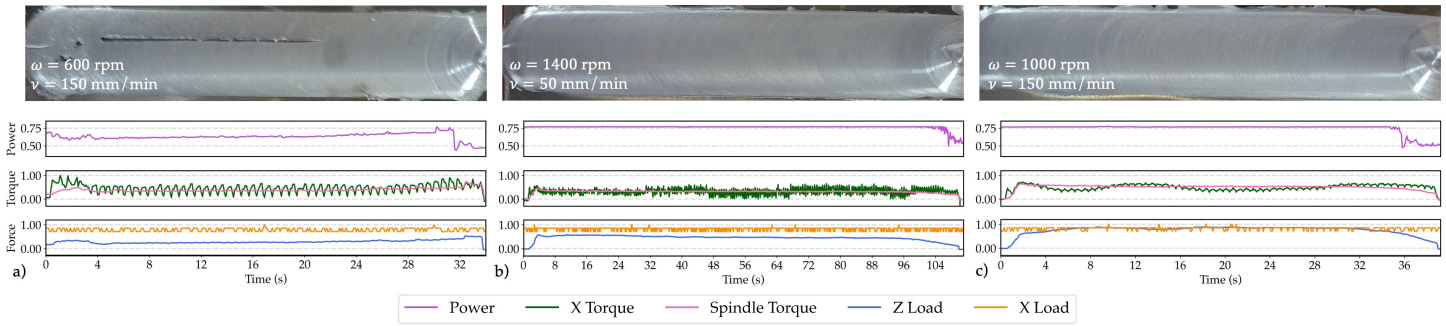

FIGURE 3: POWER, TORQUE, AND FORCE SIGNALS COLLECTED DURING THE FABRICATION PROCESS FOR WELD SPECIMENS IN VARIOUS QUALITY OUTCOMES: A) A LOW-QUALITY SPECIMEN, B) A MEDIUM-QUALITY SPECIMEN, AND C) A HIGH-QUALITY SPECIMEN.

- High tensile strength (Good quality weld, labeled as High): Parts with UTS that is above 202.5 MPa, i.e., value corresponds to 75% and above the base material's strength.

Note that the base material's strength is 270 MPa. Figure 2 illustrates the UTS value collected from each welding sample with the different parametric combinations in the experiment. Data is annotated with their assigned group according to the criteria discussed above, where circles in green represent the specimens of poor-quality weld, blue triangles correspond to the specimens of mid-quality weld, and purple squares indicate the specimens of the high-quality weld. It can be seen that the mid-quality weld parts have a lower welding speed and a lower rotational speed compared to the other two groups. As welding speed increases, the quality of welding becomes better. However, further increments in the welding speed might result in part of low weld quality. High values of ν together with the deficiency of frictional heat, will result in defective welds. Overall, no particular trend has been found between the increment of ω and ν and the increment of UTS value. The motivation of this research is to identify the combination of parameters that will yield the maximum UTS for production. Further, Figure 3 demonstrates the collected data from multiple sensors for the welding specimen of different quality outcomes. We scale all inputs to the range of $[0, 1]$ based on their corresponding maximum values.

In Figure 3 a), the specimen of $\omega = 600$ rpm and $\nu = 150$ mm/min has a low quality according to its UTS value. Multiple quality issues (i.e., void and continuous line defects) can be observed in the image of the final build. Signals collected from $\omega = 1400$ rpm and $\nu = 50$ mm/min specimen is shown in Figure 3 b) and from a high value UTS specimen are presented in Figure 3 c) $\omega = 1000$ rpm and $\nu = 150$ mm/min. Overall, it can be observed that the amplitude of Z load (line in blue) is significantly related to the quality outcome. The bigger the value, the better the weld quality. When the value of Z load is low, the weld specimen is likely to result in a continuous line defect. Also, the deviation in X torque is large in parts with smaller UTS than specimens with higher UTS values, and the power is low when generating the part with lower quality. As the next step, process information acquired from multiple sensors is fused with the proposed HCC framework for supervised learning tasks to investigate the relationship between process data and resulting quality outcomes.

4. EXPERIMENTAL RESULTS

As mentioned in Section 3, the welding speed is set to various levels in our experiment. The faster the speed of welding, the shorter the welding process will take. Therefore, the shorter length of the collected signal vectors. It takes less time to weld the specimen with a welding speed of 200 mm/min in comparison with a speed of 40 mm/min. We use *number-dash-number* format to represent the fabricated specimen in the further text for a simplified representation. The first number represents rotational speed, and the second number shows the welding speed. For example, the length of the $600-40$ specimen is five times longer than the $600-200$ specimen. To ensure all input data has the same length, we first perform sampling of the collected signals.

Figure 5 illustrates the proposed sampling procedure. Assume the length of the signal collected from the welding process M and the length of the sample is determined to be L. Therefore, the total number of the sampled signal is calculated as $M' = \lfloor M/L \rfloor$. We treat M' as step size and generate the new signal every M' step. For example, the first sampled signal is consist of 1^{st}, $M' + 1^{th}$, $2M' + 1^{th}$, ..., $(L-1)M' + 1^{th}$ digits from the original signal. In total, M' number of data will be sampled from the original data and, at the same time, keep the shape of the original signal.

We compare the HCC framework performance for the signal length of 50, 100, 150, and 200, respectively. We report the accuracy, precision, recall, and F1-score for each experiment. For different frequencies of sampling, we separate 80% of the data as training data and 20% of data for the testing set for comparison and selection of the best sampling strategy, and the experiment is replicated 50 times. We also compare the HCC effectiveness of using data from a single sensor to data from multiple sensors. Denote true positive, false positive, true negative, and false negative as TP, FP, TN, and FN, respectively. The accuracy, precision, recall, and F1 score can be calculated as

$$\text{precision} = \frac{TP}{TP + FP} \tag{4}$$

$$\text{recall} = \frac{TP}{TP + FN} \tag{5}$$

$$\text{F1 Score} = \frac{2 \times \text{precision} \times \text{recall}}{\text{precision} + \text{recall}} \tag{6}$$

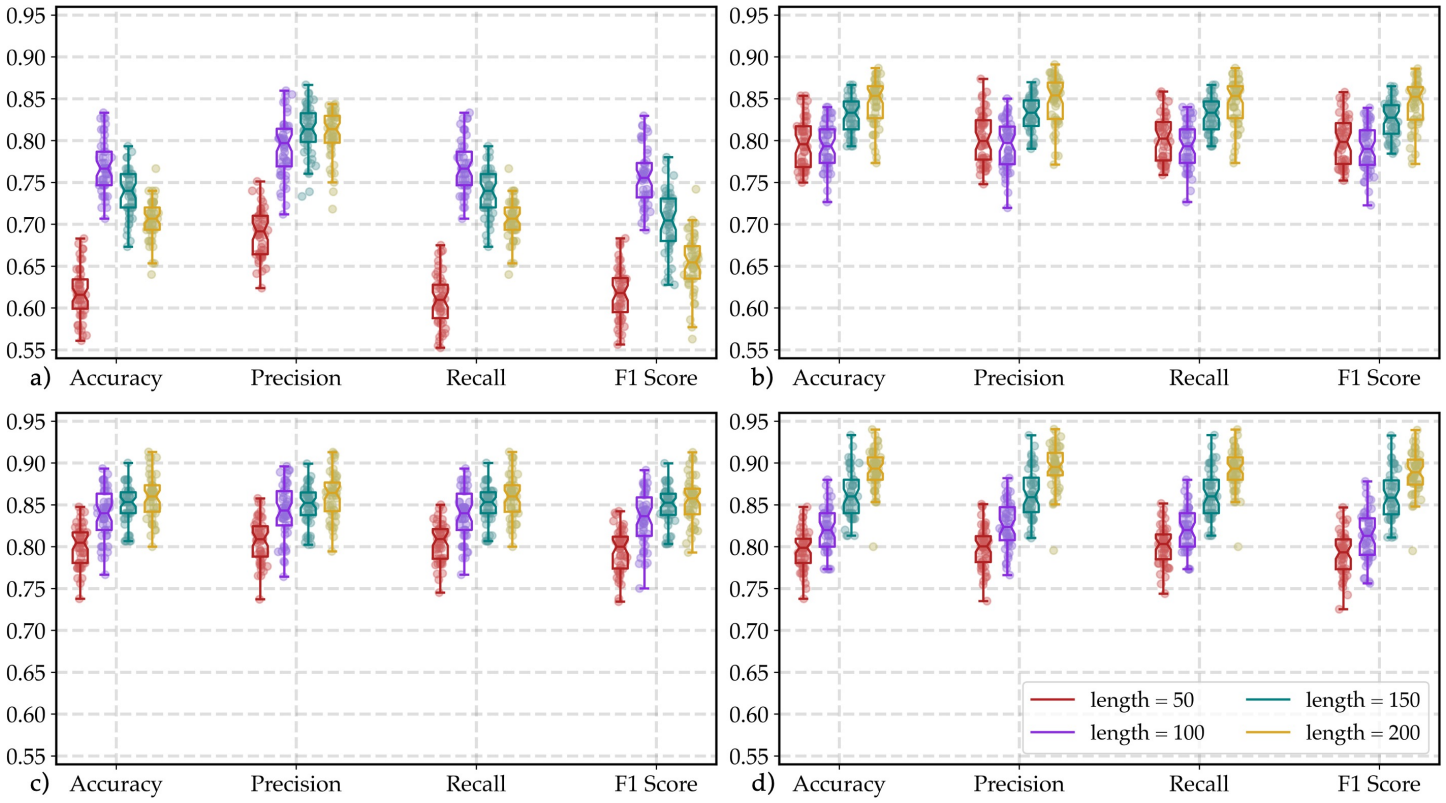

FIGURE 4: HCC FRAMEWORK PERFORMANCE FOR MULTIPLE SIGNAL LENGTHS (I.E., 50, 100, 150, 200) WHEN A) ONLY POWER DATA IS CONSIDERED, B) ONLY TORQUE DATA IS CONSIDERED, C) ONLY FORCE DATA IS CONSIDERED, AND D) POWER, TORQUE, AND FORCE DATA ARE ALL CONSIDERED. MODEL ACCURACY, PRECISION, RECALL, AND F1-SCORE ARE REPORTED.

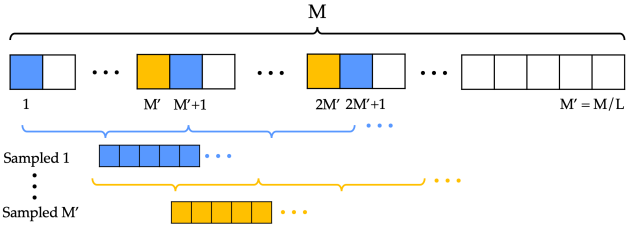

FIGURE 5: ILLUSTRATION OF SAMPLING A SIGNAL.

where accuracy shows the power of the proposed methodology to diagnose TP and TN correctly. Precision identifies the positives that are found precisely over all positive predictions. The recall is related to how many true positives the model can capture as positive, and F1-score is a function of precision and recall.

Figure 4 shows the HCC results on training with multiple signal lengths and different sensing sources. Figure 4 a), b), c), and d) shows the performance comparison of only power data considered, only torque data considered, only force data considered, and all data fused considered, respectively. In Figure 4 a), the performance metrics (accuracy, precision, recall, and F1-score) significantly increases when the length of a signal increase from 50 to 100. The framework does not perform well as the length keeps rising. This could be because the step size is too big to preserve the pattern information in power data. However, the power signal does not show extensive information related to building quality compared to torque and force data regarding its poor performance, regardless of the signal length. When only torque data is considered, HCC provides better results. For example, when the length of signal is 200, the average accuracy of the model improved from 0.704 to 0.844. When only force data is considered (see Figure 4 c)), this average accuracy is further slightly increased to 0.859. In the last case where all data sources are fused (see Figure 4 d)), the HCC framework gives the best result when data from all sources are fused for training compared to only single sensing data being used. For example, the average accuracy is 0.891 when the length equals 200. Also, the model performs better as the length of signal is longer. For example, the average F1-scores among all iterations increases are 0.790, 0.812, 0.861, and 0.888 for signals of length 50, 100, 150, 200, respectively. As a result, we select fused data with a length of 200 for further analysis. Next, data augmentation method (i.e., jittering) is implemented to balance classes from all classes. We jitter the data of each class to match the number of the class with the most data. Finally, we compare the proposed HCC with other conventional supervised learning models such as support vector machine (SVM), logistic regression (LR), Naive-Bayes (NB), and multilayer perceptron (MLP). Again, 80% of the data is selected for training and 20% for testing, and each algorithm is implemented 50 times. The averaged accuracy, precision, recall, and F1-score are summarized in Table 2.

The proposed HCC provides an accuracy of 0.902 ± 0.045, precision of 0.915 ± 0.038, recall of 0.902 ± 0.045, and F1 score of

TABLE 2: ACCURACY, PRECISION, RECALL, AND F1 SCORE OF THE PROPOSED HCC COMPARED TO OTHER MACHINE LEARNING METHODS.

Model	Accuracy	Precision	Recall	F1 Score
HCC	0.902 ± 0.045	0.915 ± 0.038	0.902 ± 0.045	0.899 ± 0.048
SVM	0.712 ± 0.125	0.747 ± 0.137	0.712 ± 0.125	0.683 ± 0.123
LR	0.537 ± 0.132	0.410 ± 0.150	0.537 ± 0.131	0.421 ± 0.150
NB	0.885 ± 0.043	0.910 ± 0.029	0.885 ± 0.043	0.879 ± 0.048
MLP	0.359 ± 0.081	0.205 ± 0.029	0.359 ± 0.081	0.217 ± 0.048

TABLE 3: MODEL PARAMETER SETTINGS AND MODEL STRUCTURE UTILIZED FOR COMPARISON.

Model	Parameters
SVM	Max Iterations = 1, Kernel Function = Radial basis function
LR	Max Iterations = 1, Solver = Limited-memory Broyden-Fletcher-Goldfarb-Shanno
NB	Additive Smoothing = 1.0
MLP	Max Iterations = 1, No. of Layers = 2, No. of Hidden Neurons = 100, Solver = Adam

0.899 ± 0.048 in 50 iterations. It can be observed that HCC provides a better result in comparison with other conventional learning methods. Regarding the accuracy, HCC improves 19.000%, 36.524%, 1.667%, and 54.333% compared to SVM, LR, NB, and MLP, respectively. Similarly, HCC performs 21.579%, 47.779%, 1.933%, and 68.139% better than SVM, LR, NB, and MLP regarding the F1-score. Overall, the experimental result shows that the proposed HCC framework provides comparable performance to other state-of-the-art methods and shows strong potential in understanding welding process-property relationships with limited data. At the end, parameters used for each learning model are summarized in Table 3.

5. CONCLUSIONS

Despite the recent studies of machine learning based methods for process-property characterization and determining defective and non-defective joints in friction stir welding (FSW), lack of interpretability, poor accuracy, and low sample efficiency prevent trustworthy analysis. We introduce hyperdimensional computing (HCC) as a cognitive solution that fuses the in-process power, torque, and force data to connect the process parameters with ultimate tensile strength. HCC not only learns the process-property relationships with few iterations and limited data but also introduces interpretability and robustness into computation using the notion of holographic representation and brain-inspired operations such as bundling and binding. Data augmentation is integrated to tackle the issue with the unbalanced data. The experimental results of a real-world case study show that HCC links the multi-channel data to ultimate tensile strength with 0.902 ± 0.045, precision of 0.915 ± 0.038, recall of 0.902 ± 0.045, and F1 score of 0.899 ± 0.048 in 50 iterations. Our future work will focus on capturing heterogeneous defects localization through cognitive learning.

REFERENCES

[1] Burford, Dwight, Widener, Christian and Tweedy, Bryan. "Advances in friction stir welding for aerospace applications." *6th AIAA Aviation Technology, Integration and Operations Conference (ATIO)*: p. 7730. 2006.

[2] Trinh, Dao, Frappart, Simon, Rückert, Guillaume, Cortial, François and Touzain, Sébastien. "Effect of friction stir welding process on microstructural characteristics and corrosion properties of steels for naval applications." *Corrosion Engineering, Science and Technology* Vol. 54 No. 4 (2019): pp. 353–361.

[3] Kawasaki, Takeshi, Makino, Toshiaki, Masai, Kentarou, Ohba, Hideshi, Ina, Yoshihiko and Ezumi, Masakuni. "Application of friction stir welding to construction of railway vehicles." *JSME International Journal Series A Solid Mechanics and Material Engineering* Vol. 47 No. 3 (2004): pp. 502–511.

[4] Hori, H and Hino, H. "Application of friction stir welding to the car body." *Welding international* Vol. 17 No. 4 (2003): pp. 287–292.

[5] Mishra, Rajiv S and Ma, ZY. "Friction stir welding and processing." *Materials science and engineering: R: reports* Vol. 50 No. 1-2 (2005): pp. 1–78.

[6] He, Xiaocong, Gu, Fengshou and Ball, Andrew. "A review of numerical analysis of friction stir welding." *Progress in Materials Science* Vol. 65 (2014): pp. 1–66.

[7] Mishra, Debasish, Roy, Rohan Basu, Dutta, Samik, Pal, Surjya K and Chakravarty, Debashish. "A review on sensor based monitoring and control of friction stir welding process and a roadmap to Industry 4.0." *Journal of Manufacturing Processes* Vol. 36 (2018): pp. 373–397.

[8] Podržaj, Primož, Jerman, Boris and Klobčar, Damjan. "Welding defects at friction stir welding." *Metalurgija* Vol. 54 No. 2 (2015): pp. 387–389.

[9] Das, Bipul, Pal, Sukhomay and Bag, Swarup. "A combined wavelet packet and Hilbert-Huang transform for defect detection and modelling of weld strength in friction stir welding process." *Journal of Manufacturing Processes* Vol. 22 (2016): pp. 260–268.

[10] Longhurst, William R, Wilbur, Isaac C, Osborne, Brandon E and Gaither, Bryan W. "Process monitoring of friction stir welding via the frequency of the spindle motor current." *Proceedings of the Institution of Mechanical En-*

gineers, Part B: Journal of Engineering Manufacture Vol. 232 No. 4 (2018): pp. 720–730.

[11] Verma, Shubham, Gupta, Meenu and Misra, Joy Prakash. "Performance evaluation of friction stir welding using machine learning approaches." *MethodsX* Vol. 5 (2018): pp. 1048–1058.

[12] Sudhagar, S, Sakthivel, M and Ganeshkumar, P. "Monitoring of friction stir welding based on vision system coupled with Machine learning algorithm." *Measurement* Vol. 144 (2019): pp. 135–143.

[13] Thapliyal, Shivraman and Mishra, Akshansh. "Machine learning classification-based approach for mechanical properties of friction stir welding of copper." *Manufacturing Letters* Vol. 29 (2021): pp. 52–55.

[14] Hartl, R, Praehofer, B and Zaeh, MF. "Prediction of the surface quality of friction stir welds by the analysis of process data using Artificial Neural Networks." *Proceedings of the Institution of Mechanical Engineers, Part L: Journal of Materials: Design and Applications* Vol. 234 No. 5 (2020): pp. 732–751.

[15] Maleki, E. "Artificial neural networks application for modeling of friction stir welding effects on mechanical properties of 7075-T6 aluminum alloy." *IOP Conference Series: Materials Science and Engineering*, Vol. 103: p. 012034. 2015. IOP Publishing.

[16] Verma, Shubham, Misra, Joy Prakash and Popli, Dipesh. "Modeling of friction stir welding of aviation grade aluminium alloy using machine learning approaches." *International Journal of Modelling and Simulation* Vol. 42 No. 1 (2022): pp. 1–8.

[17] Vabalas, Andrius, Gowen, Emma, Poliakoff, Ellen and Casson, Alexander J. "Machine learning algorithm validation with a limited sample size." *PloS one* Vol. 14 No. 11 (2019): p. e0224365.

[18] Imani, Farhad, Chen, Ruimin, Diewald, Evan, Reutzel, Edward and Yang, Hui. "Deep learning of variant geometry in layerwise imaging profiles for additive manufacturing quality control." *Journal of Manufacturing Science and Engineering* Vol. 141 No. 11 (2019): p. 111001.

[19] Ge, Lulu and Parhi, Keshab K. "Classification using hyperdimensional computing: A review." *IEEE Circuits and Systems Magazine* Vol. 20 No. 2 (2020): pp. 30–47.

[20] Zou, Zhuowen, Kim, Yeseong, Imani, Farhad, Alimohamadi, Haleh, Cammarota, Rosario and Imani, Mohsen. "Scalable edge-based hyperdimensional learning system with brain-like neural adaptation." *Proceedings of the International Conference for High Performance Computing, Networking, Storage and Analysis*: pp. 1–15. 2021.

[21] Zou, Zhuowen, Alimohamadi, Haleh, Zakeri, Ali, Imani, Farhad, Kim, Yeseong, Najafi, M Hassan and Imani, Mohsen. "Memory-inspired spiking hyperdimensional network for robust online learning." *Scientific Reports* Vol. 12 No. 1 (2022): p. 7641.

[22] Chen, Ruimin, Imani, Mohsen and Imani, Farhad. "Joint active search and neuromorphic computing for efficient data exploitation and monitoring in additive manufacturing." *Journal of manufacturing processes* Vol. 71 (2021): pp. 743–752.

[23] Imani, Farhad and Chen, Ruimin. "Latent Representation and Characterization of Scanning Strategy on Laser Powder Bed Fusion Additive Manufacturing." *ASME International Mechanical Engineering Congress and Exposition*, Vol. 86649: p. V02BT02A009. 2022. American Society of Mechanical Engineers.

[24] Chen, Ruimin, Sodhi, Manbir, Imani, Mohsen, Khanzadeh, Mojtaba, Yadollahi, Aref and Imani, Farhad. "Brain-inspired computing for in-process melt pool characterization in additive manufacturing." *CIRP Journal of Manufacturing Science and Technology* Vol. 41 (2023): pp. 380–390.

[25] Rashid, Khandakar M and Louis, Joseph. "Times-series data augmentation and deep learning for construction equipment activity recognition." *Advanced Engineering Informatics* Vol. 42 (2019): p. 100944.